Soils and Foundations 2013;53(4):510–524

The Japanese Geotechnical Society

Soils and Foundations

www.sciencedirect.com
journal homepage: www.elsevier.com/locate/sandf

Disk shaped piezo-ceramic transducer for P and S wave measurement in a laboratory soil specimen

Laxmi Prasad Suwal, Reiko Kuwano*

Institute of Industrial Science, The University of Tokyo, Tokyo, Japan

Received 25 October 2011; received in revised form 21 March 2013; accepted 3 May 2013
Available online 29 July 2013

Abstract

Piezo-ceramic elements are customized as transducers for the measurement of mechanical properties of materials in the engineering field. This was made possible with the industrial production of piezo-ceramic elements in various shapes and sizes. This paper describes the development of a single flat disk shaped piezo-ceramic transducer for measuring both compression and shear wave on an identical soil specimen. Procedures for interpreting results, initial verifications of its performance and applications are also presented. Two types of piezo-ceramic elements, one for measuring P waves and the other for S waves, were placed together in a metal housing, which worked as a wave measuring transducer installed in a triaxial apparatus. Three kinds of granular geo-materials, fine, medium-coarse and coarse sands, were tested. Small strain shear stiffness, G_{max}, of the tested sands was evaluated by various techniques, including proposed disk transducer method, trigger and accelerometer method and traxial small strain cyclic loading. Shear moduli obtained from all the techniques fell in a similar range within allowable scatters and it was confirmed that the disk transducer was one of applicable wave measurement technique for laboratory soil specimens.

Keywords: Laboratory test; Sands; Small strain stiffness; Elastic wave measurement; Piezo-ceramic transducer(IGC: D07)

1. Introduction

Accurate evaluation of small strain stiffness of the soil is essential for reliable structures analysis and the prediction of deformation when subjected to static and dynamic loading. Several researchers have attempted to develop a reliable technique for measuring local strain, with inclinometers (Burland and Symes, 1982; Ackerley et al., 1987), hall-effects (Clayton and Khatrush, 1986), LDTs (Goto et al., 1991), non-contact transducers (Hird and Yung, 1989; Hicher, 1996; Di Benedetto and Tatsuoka, 1997), fiber optics (Lee et al., 2011) among them. Local strain is measured to avoid the effects of bedding errors and system compliance (Tatsuoka and Shibuya, 1992; Lo Presti et al., 1993; Tatsuoka et al., 1994; Tatsuoka and Kohata, 1995). The tangent modulus at such small strain level is known as the small strain stiffness modulus, which is assumed to be elastic, recoverable, independent of strain level and is measurable by the velocities of elastic waves propagating through the material (Richart et al., 1970; Jardine et al., 1984; Burland 1989; Tatsuoka and Shibuya, 1992; Arroyo et al., 2003). One of the merits of using elastic waves for such a purpose, and in particular, shear waves, is that the measurement can be performed on a laboratory specimen in a non-destructive manner and in the course of other testing procedures (such as triaxial tests, etc.). Another is that it is possible to make a direct comparison between the field and laboratory data. Seismic shear wave measurements have been used in the field such as PS logging, Cross-hole, Down-hole and Up-hole method since the early works of Stokoe and Hoar (1978) and Stokoe and Santamarina (2000).

*Corresponding author.
E-mail address: kuwano@iis.u-tokyo.ac.jp (R. Kuwano).
Peer review under responsibility of The Japanese Geotechnical Society.

Production and hosting by Elsevier

0038-0806
http://dx.doi.org/10.1016/j.sandf.2013.06.004

Several laboratory techniques for the measurement of elastic waves have been used in geotechnical laboratories. Shirley and Hampton (1978), the first to propose the Bender Element method, were pioneers. After this work, their technique was extensively used in various testing apparatus, including the oedometer (Jamiolkowski et al., 1995; Lee et al., 2010), triaxial apparatus (Viggiani and Atkinson, 1995; Jovicic et al., 1996), torshional shear apparatus (Duttine et al. 2007; Mulmi, 2008) and in resonant columns (Camacho-Tauta et al., 2008). The Bender Element method allowed last of these direct and well controlled comparisons between diverse dynamically measured elastic properties. Another method of measuring propagated waves in the specimen proposed in the University of Tokyo is known as trigger accelerometer method (Ahn Dan and Koseki, 2002). In this method, a pair of triggers is firmly installed on the top cap, which is excited according to the function set on the function generator (various types of signals in terms of wavelet form and frequency can be used as required). A pair of accelerometers is fixed on the surface of the specimen as schematically shown in Fig. 1. This technique was simultaneously employed in this study, and made it possible to directly compare the results with the proposed method of wave measurement. Other significant works of using accelerometer of piezoelectric transducers as receivers includes Pallara et al. (2008) and Camacho-Tauta et al. (2008).

Nowadays, the Bender Element is the most commonly used technique among the wave measurement techniques for in the laboratory soil specimens, due to its simplicity and relatively low cost. However, it may not be suited to undisturbed or cemented materials (Amaral et al., 2011; Pineda et al., 2008), as it is always necessary to insert the element into the specimen, which may cause significant disturbance in the vicinity of the insert. Because the surface shape of the disk transducer is flat, it can be applied to various types of specimens, including stiff or cemented materials, with relative ease. A disk transducer can measure compression and shear waves in an identical specimen. Generally, the Bender Element is used to measure only shear wave velocity. A number of researchers have measured compression and shear waves in a single specimen using a compression plate for compression wave and Bender Element for shear wave (Brignoli et al., 1996; Lee et al., 2010). Recently, a Bender-Extender was developed for measuring both compression and shear waves (Leong et al., 2009; Kumar and Madhusudhan, 2010). There are limited studies on using a flat plate for the transmission and receiving shear wave (Brignoli et al., 1996; Ismail and Rammah, 2005). Besides this work, we have published our results on a single transducer for measuring both compression and shear waves in a single specimen.

This paper presents the configuration of the transducer, and explains the calibration method, and how to process and interpret the signals. The performance is displayed by the test results on three kinds of granular materials. The small strain stiffness interpreted by the disk transducer method was compared with those obtained by the trigger accelerometers technique and small cyclic loadings.

2. Disk transducer for P and S wave measurement

2.1. Piezoelectric element and disk transducer

A piezoelectric element generates an electric charge on the application of stress and deformation occurs on the application of the electric voltage. This property is called the piezoelectric effect. By virtue of this effect, piezoelectric elements are extensively used as transducers in many fields, including

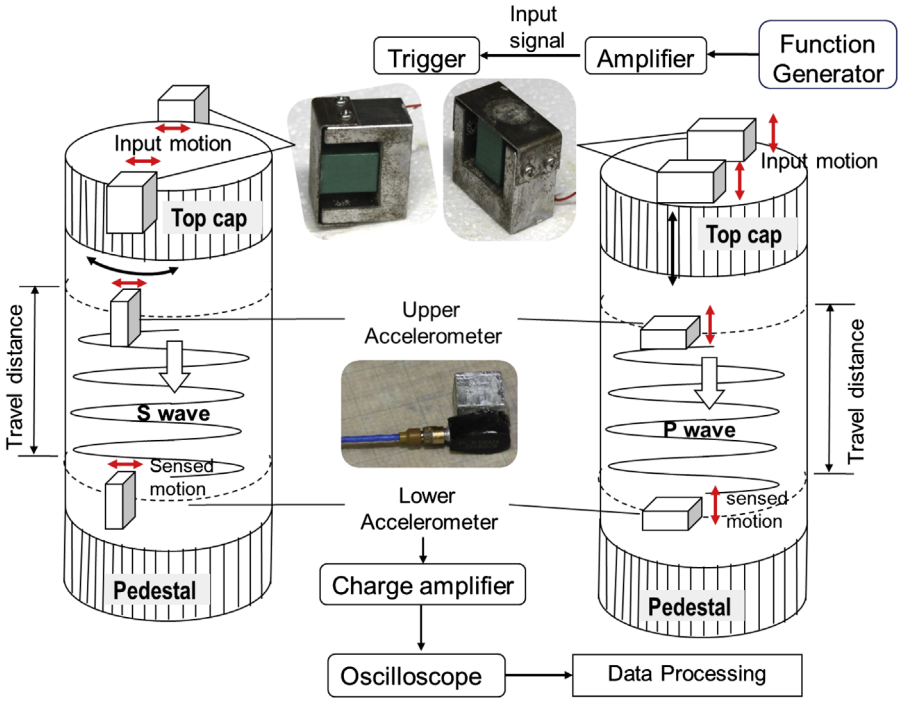

Fig. 1. Trigger accelerometer method. (a) P-type piezo element and (b) S-type piezo element.

engineering. Industrially produced flat shaped piezoelectric elements were used in this study. Two types of piezo-ceramic elements are commercially available, a P-type element and an S-type element. The P-type element is polarized in the perpendicular direction to the electrode in the longitudinal direction, so it generates a compression (P) wave upon the application of voltage. Conversely, the S-type element is polarized in the parallel direction to the electrode in the transverse direction, generating a shear (S) wave. Schematic figures of P and S type piezo-ceramic elements are shown in Fig. 2a and b, respectively. The piezo-ceramic elements of lead zirconate titanate materials [$Pb(Ti.Zr)O_3$] were applied. The properties of these piezo-ceramic elements are displayed in Table 1. P-type (diameter: 20 mm, thickness: 2 mm) and S-type (diameter: 20 mm, thickness: 5 mm) elements were adapted to the transducer suited to the sample having diameter of 75 mm and height of 150 mm. The PS-type element, which can emit and receive both compression and shear waves, was

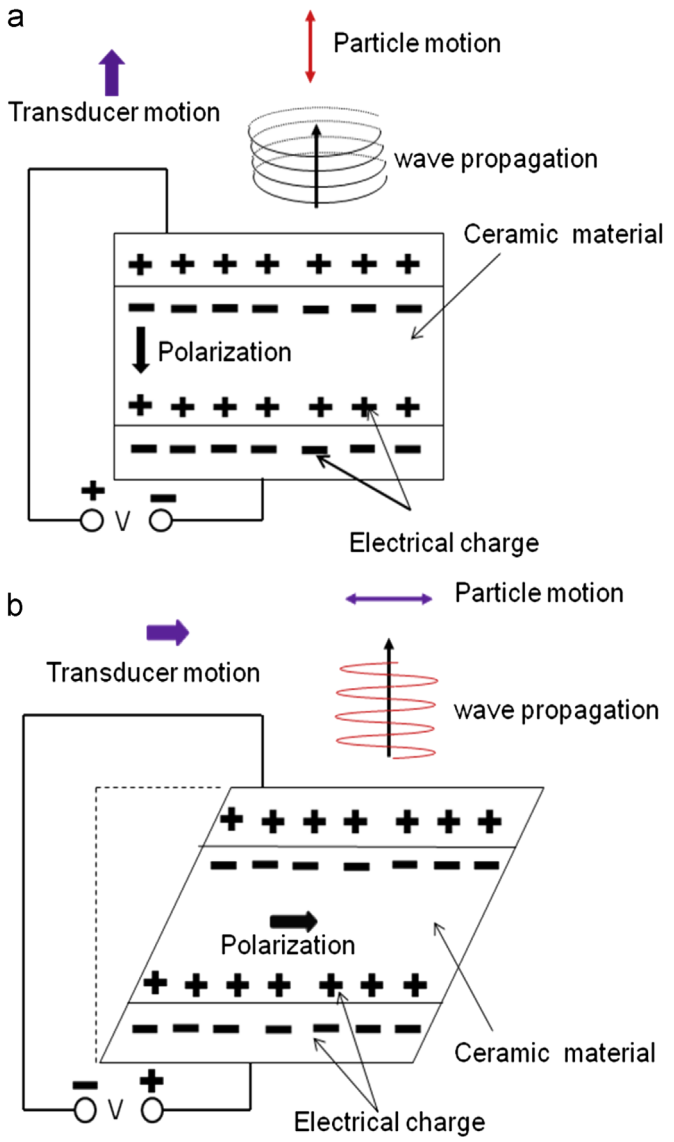

Fig. 2. Schematic figures of piezo element. (a) P-type piezo element and (b) S-type Piezo element.

Table 1
Properties of used piezo-ceramic elements.[a]

S.N	Z2T20D-SYX (C-6)—P-type				SZ5T20D-LLYX (C-6)—S-type			
	Kp[b] (%)	C [c] (pF)	Diameter (mm)	Thickness (mm)	K15[b] (%)	C[c] (pF)	Diameter (mm)	Thickness (mm)
1	65.6	3100	20.00	2.01	64.8	1322	20.02	4.99
2	66	3100	19.99	2.01	65.4	1339	20.02	4.99

[a]Lead zirconate titanate ceramic [$Pb(Ti.Zr)O_3$], manufactured by Fuji Ceramics Co.
[b]Kp, K15: coupling factors.
[c]C: electro static capacity.

assembled by firmly merging P-type and S-type elements in epoxy resin. Pictures of P-type, S-type and PS-type peizo-ceramic elements are shown in Fig. 3. The piezo-ceramic elements were coated with a thin layer of epoxy resin to protect them from being damaged and from water. Several differently shaped patterns of surface coating were initially considered to ensure the firm contact between the transducer and tested material. In this study, a flat surface coating was adopted because it was found to perform better than corrugated or sand-papered surfaces (Suwal et al., 2009). The thin layer of epoxy resin between the S-type and P-type elements sticks them to each other and also assures a barrier to electric conductivity. The PS-element was assembled in the metal housing which was placed in the center of the top cap and pedestal of the triaxial apparatus. A detailed sketch of the assembly of the top cap or pedestal is shown in Fig. 4. The side of the S-type element was surrounded by a 2 mm thick silicon layer which is softer than epoxy resin, in order to allow its easier shear motion. Here, we call the metal capsulated PS-type element "the PS Disk Transducer".

2.2. Calibration and working frequency range

Calibration of the whole system was required prior to the experiments. In the PS disk transducer, the S-type element is placed at the upper position and P-type at the lower position. The surface is coated by a thin layer of epoxy resin. The time required for signals to travel through ceramics and epoxy resin layers needs to be considered. It was calibrated by placing the two disk transducers in direct contact with each other, as shown in Fig. 5. To ensure the contact between the transmitter and the receiver disk transducers, they were compressed through the loading piston and the value of load was detected by a load cell. Initially a load of 39 N was applied. The P-type element of transmitter transducer was excited with single sinusoidal signals of input frequencies ranging from1 to 40 kHz and the input and output signals were recorded. Typical waveforms recorded at input frequencies of 2 kHz, 6 kHz and 10 kHz are shown in Fig. 6. The rising of signal at the transmitter and at the receiver transducer were determined and the time delay was obtained. The required time was found to be in the range of 3.7–4.3 μs. The effect of change of pressure was confirmed by increasing the load through the loading piston to be 105 N and the P waveforms obtained are

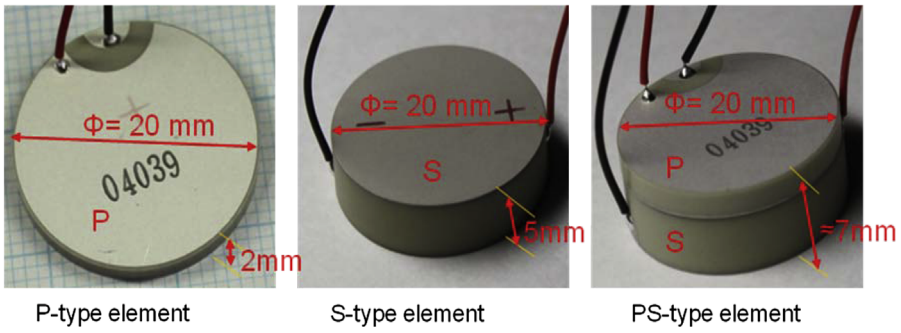

Fig. 3. Pictures of piezo-ceramic elements used in this study.

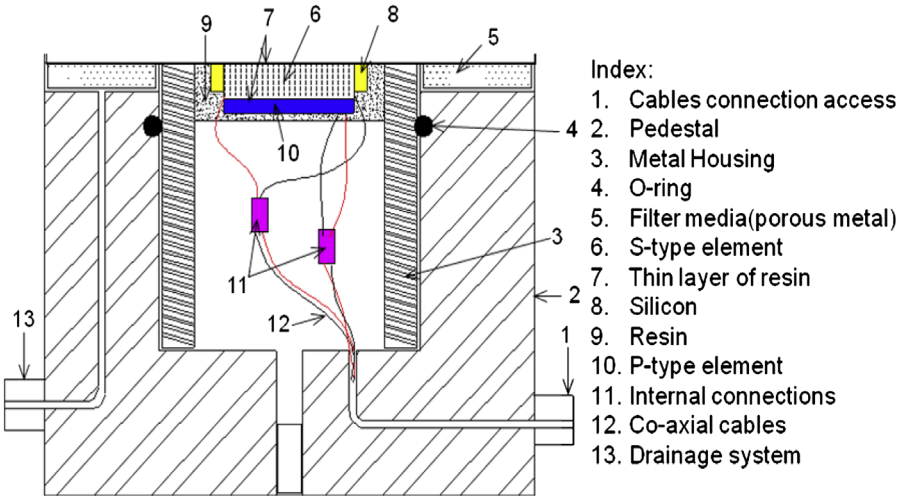

Fig. 4. Detailed sketch of pedestal including disk transducer.

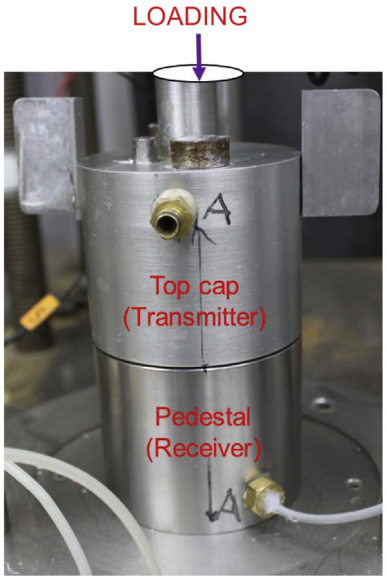

Fig. 5. Experimental set-up during calibration.

shown in Fig. 7. An analysis of the recorded data revealed that the time lag between the rising of the signal at transmitter and at receiver was in the same range as that in the case of 39 N loading. The correction value for P-wave measurement was confirmed as 4 μs regardless of input frequency and contact pressure. Similarly, the single sinusoidal signals with input frequencies of 1–40 kHz were excited through S-type piezo-ceramic element. The S waveforms recorded at input frequencies of 1–40 kHz under the axial load of 105 N are displayed in Fig. 8, showing that no correction is required for S wave measurements.

However, it was noted in Fig. 8 that the frequency of the first arrival wave at the receiver did not correspond well to that of transmitted wave at the frequencies of 10, 12, 15 and 20 kHz. In these cases, the frequencies of the received waves were 6–8 kHz in spite of the fact that frequencies of the transmitted wave were much larger. In lower and higher frequency rages, less than 8 kHz and larger than 30 kHz, the frequency of the transmitted and received wave were found to be similar. There seems to be a particular frequency range in which S waves cannot be transmitted at the specified frequencies. In this study, therefore, the measurement was carried out using the waves of frequencies lower than 8 kHz. It should be also noted that this frequency characteristics appears to depend on the structure condition of each transducer. Possible reasons for this may be that the motion of the S-element was complex due to the constraint and/or fixing condition at certain frequencies. A similar phenomenon was reported for the Bender Element. Pallara et al. (2008) found that the source bender element did not deform as assumed at high frequencies. This only happened

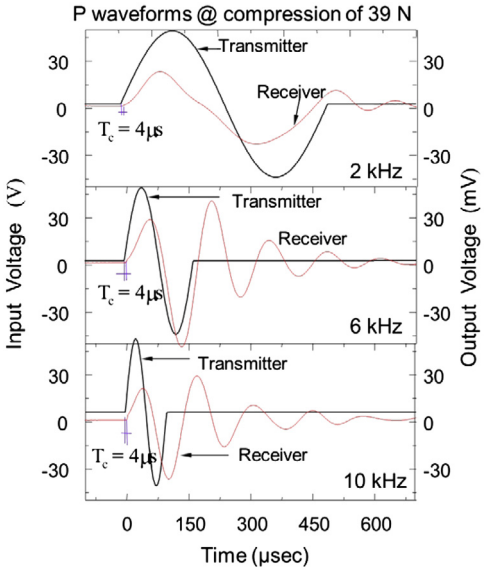

Fig. 6. Typical P waveforms during calibration (load = 39 N).

for S wave propagation. No such phenomenon was found in P wave propagation, as confirmed in Fig. 7.

3. Materials tested and apparatus

3.1. Tested materials

Three sorts of granular geo-materials, Toyoura sand, Silica sand and Hime gravel, varying grain size from 0.2 mm to 2 mm were used in this study. Toyoura sand is fine-grained, uniformly graded sand. Silica sand is composed of quartz. In this study, Silica sand with a mean diameter, D_{50}, of 0.45 mm was used. Hime gravel is poorly sorted, and the grain shape is angular. It was taken from Hime River, Otari, Kitaazumi, Nagano prefecture, Japan. It is derived from sandstone, granite, shale, quartz etc. Pictures of these materials are shown in Fig. 9. Their physical properties, including specific gravity, maximum and minimum void ratios, mean diameter and Poisson's ratio, which was later used for the shear stiffness calculation of the tested materials and gradation curves, are shown in Table 2 and Fig. 10, respectively.

3.2. Triaxial apparatus and wave measurement equipment

A small piece of gear driven and strain controlled triaxial equipment, as shown in Fig. 11, was used in the experiment. The axial loading system consists of an AC servomotor and a reduction gear system, electromagnetic clutches and brakes. Stress and strain are precisely controlled by a high speed computer. The signal for the transmitting wave was generated by a digital automatic function generator which can produce a maximum peak at a peak voltage of 10 V and is capable of producing twelve different types of waveforms at frequency ranges of 0.001 Hz–25 MHz. An amplifier was used to amplify the input signal generated by the function generator before feeding it into the transducer. An oscilloscope was used to

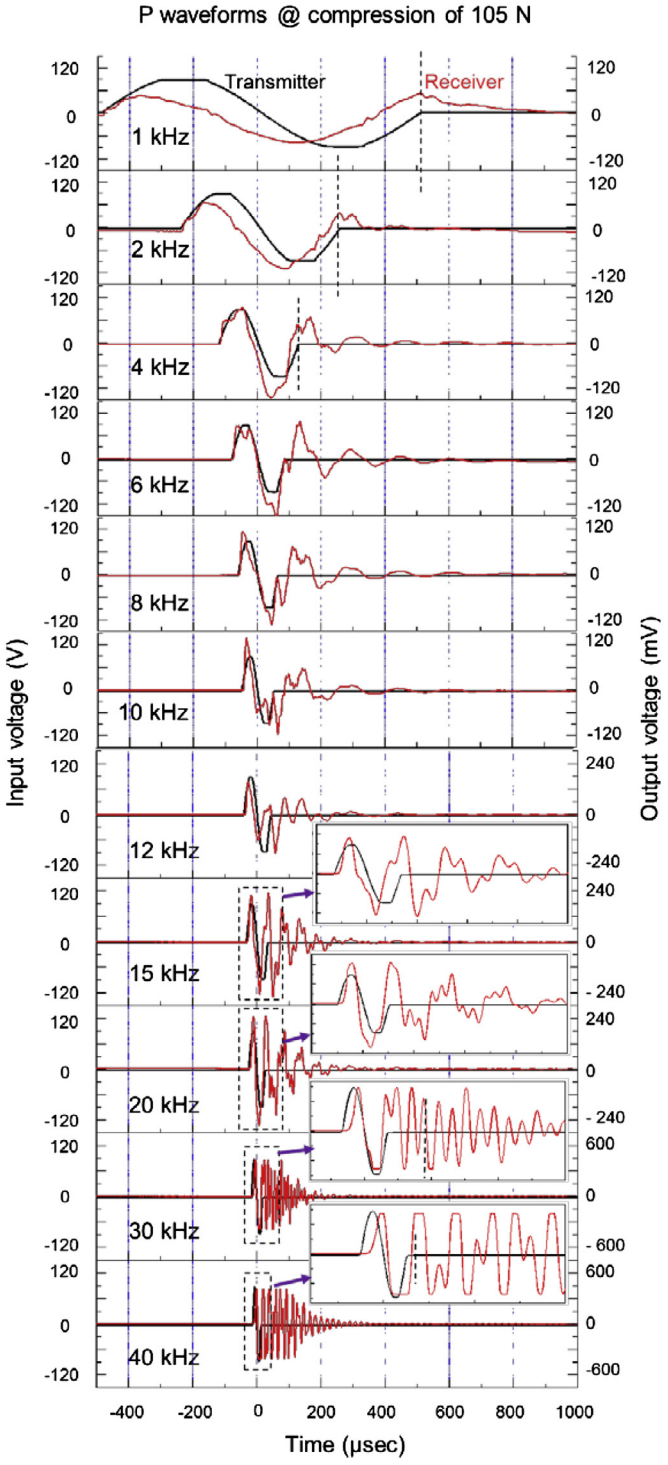

Fig. 7. Typical P waveforms during calibration (load = 105 N).

record and display waveforms of the transmitted and received signals. The features of the oscilloscope are given in Table 3.

3.3. Specimen preparation and testing procedures

The specimens used were 75 mm in diameter and 150 mm in height for all tests. The specimen was prepared by the air pluviation technique. In order to ensure constant density

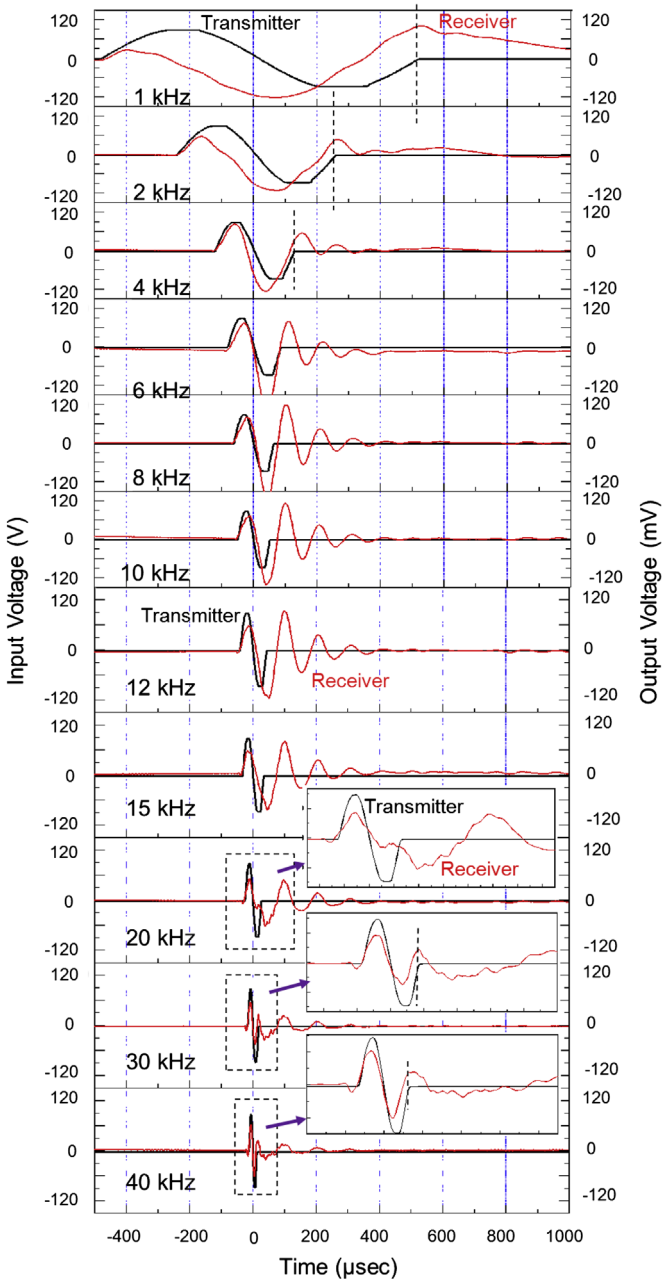

Fig. 8. Typical S waveforms during calibration (load = 105 N).

throughout the specimen, the height at which the materials were poured was kept constant. In this study, the loose specimens were prepared with a falling height of 20 cm, and an 80 cm height was maintained when preparing dense specimens. At first, the specimens were set up at an isotropic stress state of 25 kPa, and then the stress level was increased to 50, 100, 200 and 400 kPa, as shown in Fig. 12. Each specimen was kept in the stress state for a sufficient time period, for at least one hour, to allow for the dissipation of the creep effect. A total of 11 cyclic loadings with a peak to peak strain amplitude of 0.001% were applied in the vertical direction to evaluate the small strain stiffness, and another creep stage was maintained for conducting wave measurements.

Table 2
Physical and mechanical properties of tested materials.

Physical and mechanical properties	Toyoura sand	Silica sand	Hime gravel
Specific gravity, G_s	2.62	2.64	2.65
Maximum void ratio, e_{max}	0.946	0.787	0.709
Minimum void ratio, e_{min}	0.637	0.538	0.480
Mean diameter, D_{50} (mm)	0.19	0.45	1.72
Poisson's ratio	0.17	0.19	0.2

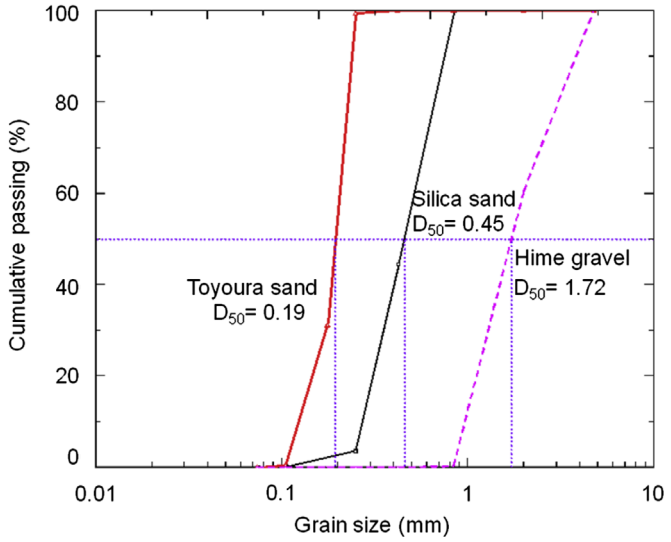

Fig. 10. Particle size distribution of tested materials.

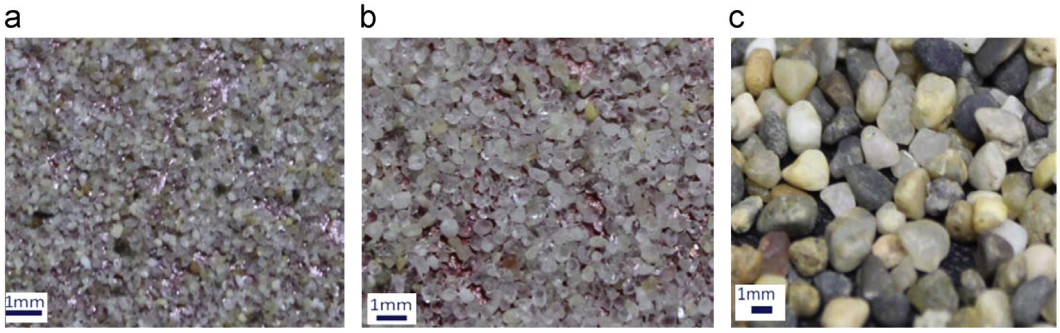

Fig. 9. Photographs of tested materials.

3.4. Test cases

Toyoura sand represented the fine grain material, Silica sand represented the medium one and Hime gravel stands were used as the coarse materials. Two tests on each material were conducted, one in loose and the other in dense state condition. The conditions of the tests are listed on Table 4, in which the information related to wave measurement is expressed with respect to disk transducer method. The wave measurements were conducted increasing the input signal from low to high frequencies. In addition to disk transducer method, trigger accelerometer method was also employed.

4. Wave velocity measurement

4.1. Signal processing adopting low pass filter

The frequency of the system noise was found to be in a range of 22–25 kHz. Then the signals were modified as the signals of frequencies lower than this were more clearly detected. The low pass filter was employed to remove waves of more than 20 kHz, considering that the system noise was a higher frequency than those of the input signals.

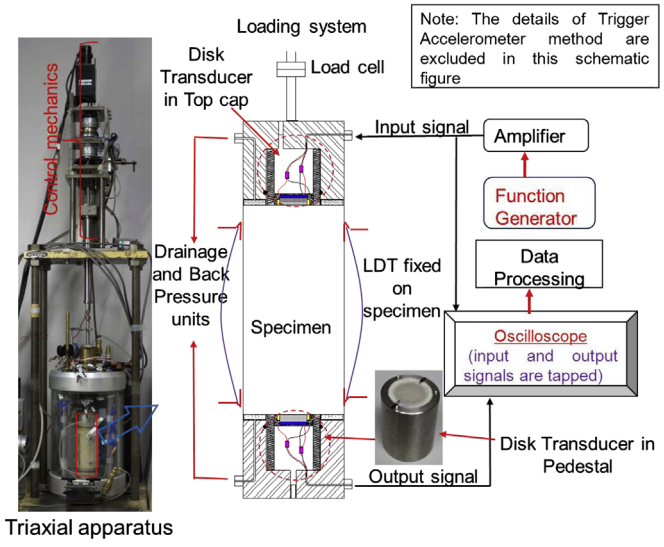

Fig. 11. Triaxial apparatus and sketch of experimental set-up.

4.2. Arrival time identification in elastic wave measurement

One of the most important issues in the elastic wave measurement is the correct determination of the arrival of signal. Compression waves produced less interesting results for discussion purposes than the shear waves, in terms of their interpretation. In case of shear waves, these are affected by (i) soil as dispersive media (Sachse and Pao, 1978), (ii) near field effect (Arroyo et al., 2003), (iii) sample geometry effect (Rio et al., 2003; Khan et al., 2011; Tallavó et al., 2011; Amaral et al., 2011), (iv) reflection on boundaries due to the sample size (Arroyo et al., 2006; Kuwano et al., 2008; Viana da Fonseca et al., 2009) and so on. A number of studies have showed that the receiver transducer sensed the complex waves consisting incident and reflected waves particularly in triaxial cylindrical specimens where the boundaries are relatively close to the source and receiver elements (Arulnathan et al., 1998; Arroyo et al. 2006). Various techniques have been proposed to minimize the uncertainties in the interpretation of the arrival time (Viggiani and Atkinson, 1995; Jovicic et al., 1996; Blewett et al., 1999; Lee and Sanatamarina, 2005; Viana da Fonseca et al., 2009). Viggiani and Atkinson (1995) suggested the use of a sinusoidal wave to reduce the uncertainties in the interpretation. The same shape signals on input and output signal could be achieved using a single sinusoidal wave as the input signal. Jovicic et al. (1996) proposed the use of a

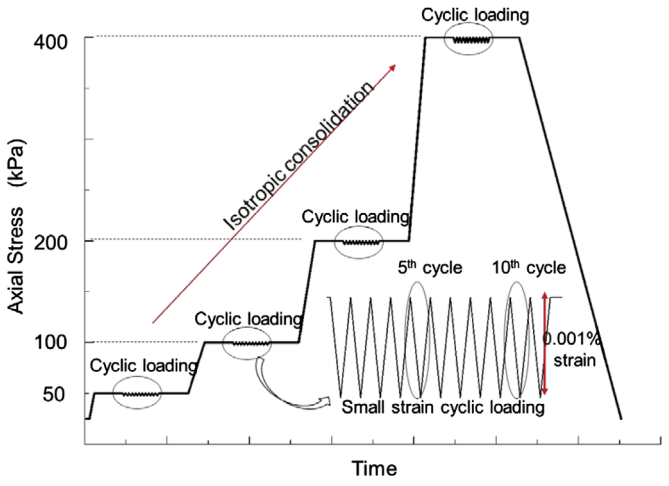

Fig. 12. Stress path of the experiment.

Table 3
Features of oscilloscope (HIOKI 8860-50).

No. of input units	Max. 4 units
No. of channels	Max. 16 analog channels (max. 64 channels with scanner unit)+16 logic channels (standard configuration)
Measurement ranges	5 mV–20 V/div, 12 ranges, (using the 8956), resolution: 1/100 of range
Max. allowable input	DC 400 V
Frequency characteristics	DC to 10 MHz
Time axis at memory function	5 μs–5 min/div, 26 ranges, sampling period: 1/100 of range, external sampling, dual time base possible
Memory capacity	12-bits × 32 M-Words/ch (1ch at 8860-50, 2ch at 8861-50) to 2 M-Words/ch (16ch at 8860-50, 32ch at 8861-50) *Memory capacity can be expanded 32 times.(Optional memory board)

Table 4
List of tests.

Test No.	Material	Relative density (%)	Specimen condition	Transducer used	Input voltage (V)	Input wave	Input frequency range (kHz)
1	Toyoura sand	56	Dry	DT&TA	±93	sine	2–30
2	Toyoura sand	92					2–30
3	Silica sand	78					2–30
4	Silica sand	99					2–30
5	Hime gravel	68					2–20
6	Hime gravel	88					2–20

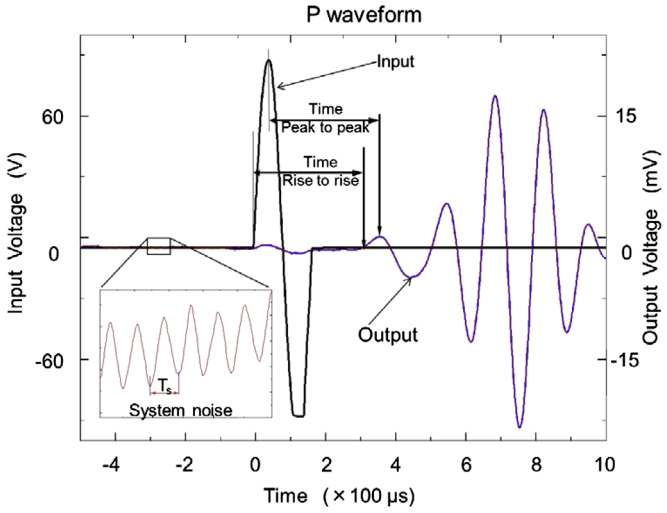

Fig. 13. Definition of travel time for compression wave.

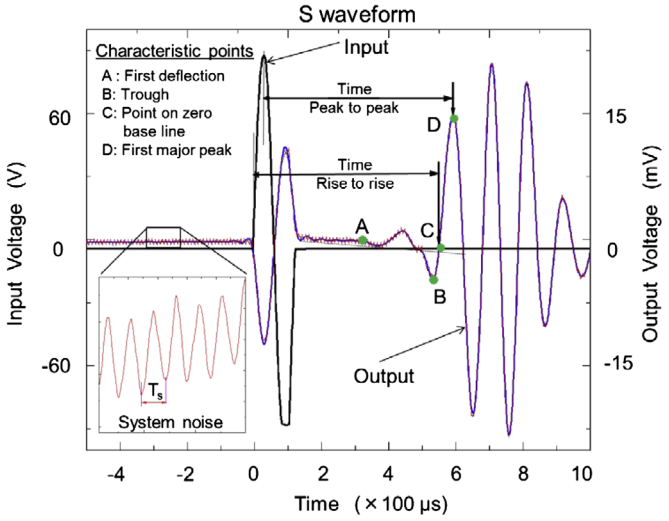

Fig. 14. Definition of travel time for shear wave.

sinusoidal wave and adoption of the point of the first inversion as the arrival of shear wave and suggested employing the high frequency signals to reduce the near field effects. Some other researchers proposed the application of characteristic points (peaks, troughs) to evaluate the travel time. The method of employing continuous sinusoidal waves has been also recently proposed (Blewett et al., 1999; Greening and Nash, 2004). The frequency of the input signal is gradually modified until input and output signals are displayed in the same phase. The measurements are repeated for different frequencies (wave lengths). The travel time is determined from the slope of a frequency vs. number of wavelengths line. The application of a methodical, systematic and objective approach for the interpretation of the results, in the time and frequency domains was proposed by Viana da Fonseca et al. (2009), and an automated tool was used to enable unbiased information to be obtained. While all the methods discussed above appear to be capable of measuring the travel time correctly under some conditions, they equally all appear to have limitations that are not well defined (Yamashita et al., 2009). Still a promising approach has arisen from using the full dynamic characterization of the specimen using the transfer function and the impulse response function (FRF, IRF), which enabled the de-convolution of the effects of the equipment, and transducers, etc. (Tallavó et al., 2011; Khan et al., 2011; Alvarado and Coop, 2011; Amaral et al., 2011)

4.3. Interpretation of signals in this study

The arrival times of compression waves were evaluated as the first deflection of the signal on time domain registers. Fig. 13 shows the typical compression waveform obtained in this study. The travel times are obtained by considering the time gap between the rising of the input signal and the rising of output signal (T_{rtr}) and the peak of the input signal and the peak of the output signal (T_{ptp}), which are clearly defined in Fig. 13.

In single sinusoidal excitation, the rising to rising travel time was defined as the distance from the rising of input signal to the first zero crossing point on the time domain of the output signal following the recommendation by Jovicic et al. (1996). The criteria employing to determine the travel times based on rise to rise of signals and peak to peak of signals are displayed in Fig. 14.

4.4. Waveforms

The continuous stacking of wave data and average of these stacked data was displayed in the monitor of the oscilloscope. In this study, the wave was excited at intervals of 1 s. The recorded waveforms were stacked and averaged continuously until the noise to signal ratio decreased to an acceptable level, so that the detection of the rising point was not affected by noise.

Figs. 15 and 16 present the typical waveforms obtained in loose Toyoura sand specimen at isotropic stress of 50 kPa and

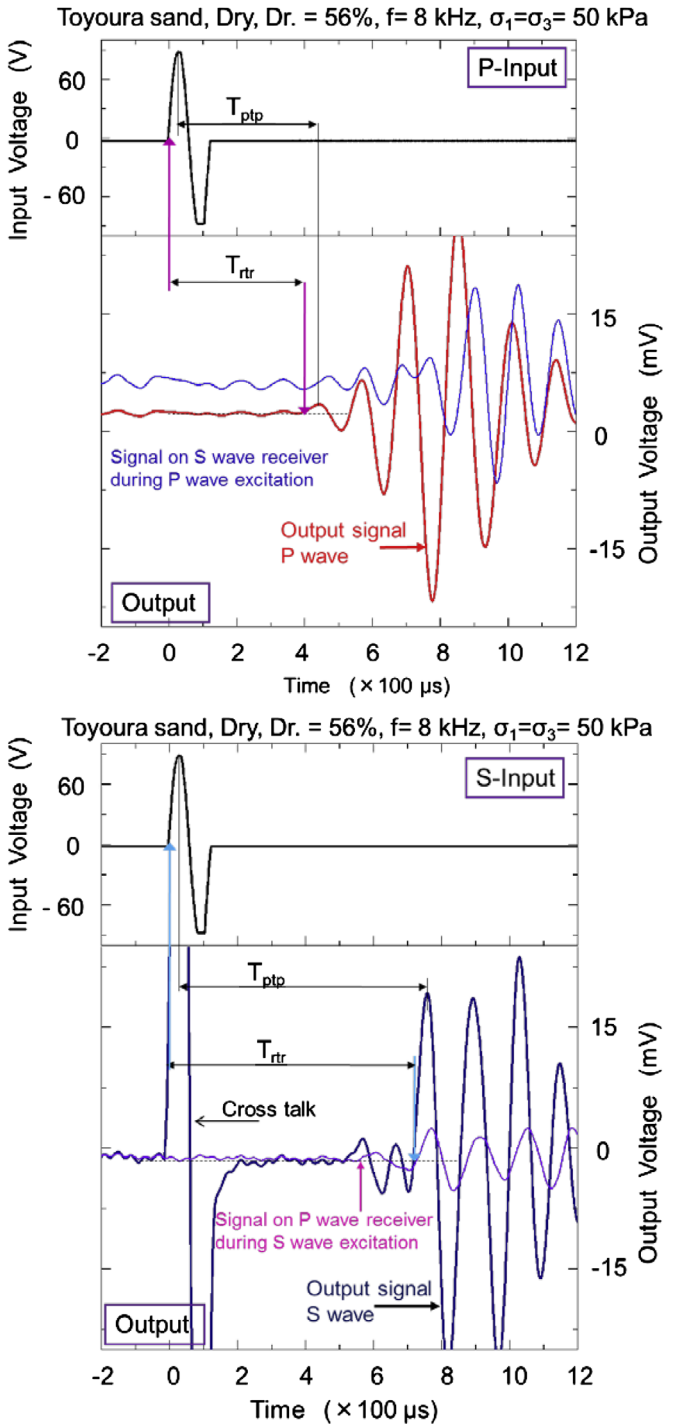

Fig. 15. Typical waveforms achieved on Toyoura sand at stress level of 50 kPa.

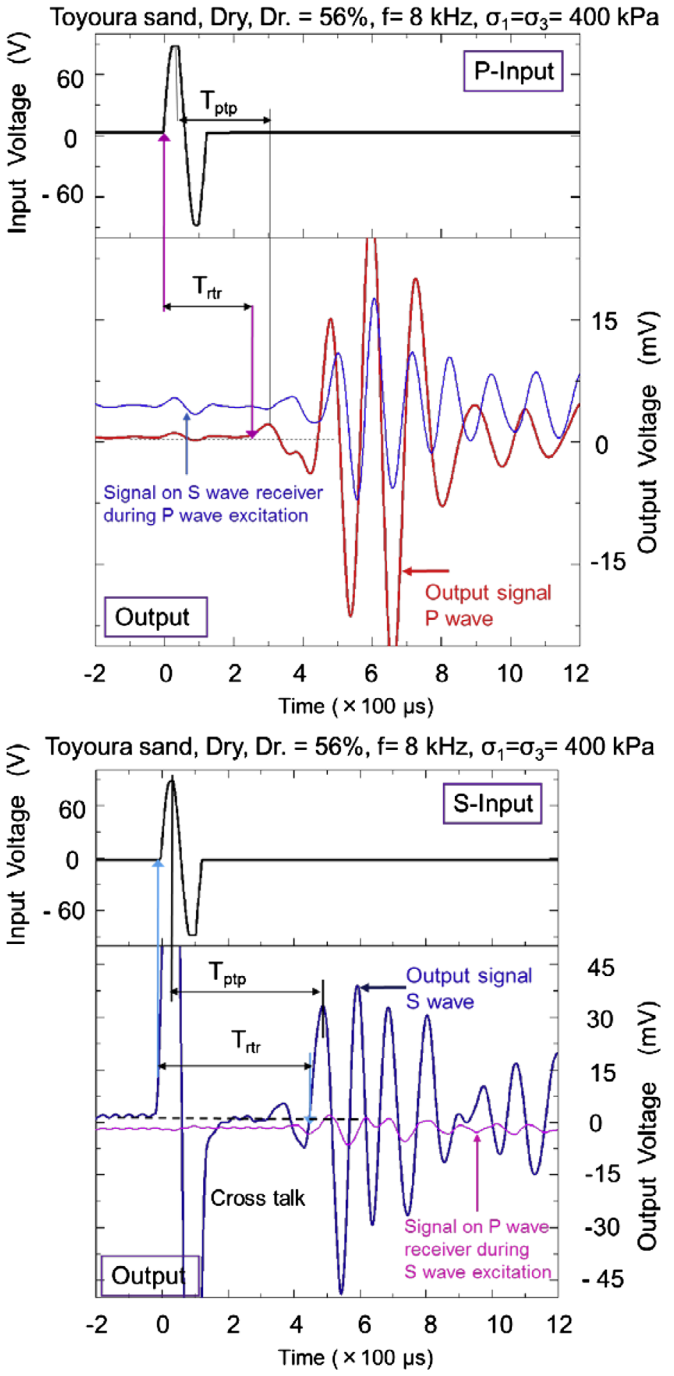

Fig. 16. Typical waveforms achieved on Toyoura sand at stress level of 400 kPa.

400 kPa respectively. A single sinusoidal wave of 8 kHz was generated through function generator and the received waves were stacked for 100–200 times in each measurement. As previously mentioned, the PS-disk transducer has the ability of sensing both compression and shear waves. The response of the S wave sensor during P wave excitation and the response of the P wave sensor during S wave excitation are also displayed in the figures. It was indicated that the propagated waves were not "perfect" P or S waves as some interference was observed between P and S elements. This, however, did not pose a serious problem in the identification of the arrival time.

Typical waveforms obtained for Silica sand and Hime gravel are shown in Figs. 17–20. In all the cases, the waveforms are clear and the rise to rise or peak to peak travel times are easily identifiable. The diameter of the sensor used in this study was 20 mm, which is approximately 10 times the mean diameter of Hime gravel. For the measurement of relatively coarse materials,

the surface contact area which transmits a wave between a sensor and tested material is considered to be sufficiently large. In this study, it was found that the measurement was successful when the diameter of the sensor was 10 times the grain size.

When one of the channels is connected to the display of the input voltage in an oscilloscope, due to the electromagnetic induction, very small signals with the same or reverse polarity and waveform may be displayed in the receiver channel simultaneously. This is called inter-channel cross-talk or simply cross talk. The polarity of the cross-talk seems to depend on the inter-channel condition and does not affect the polarity of the main wave. Sometimes, the signals encountered due to cross-talk might be problematic and be a possible source of errors especially when the arriving wave of the output and the cross-talk occur at the same time, which would make the detection of the arrival time complicated and inaccurate. The amplitude of cross-talk decreases with the distance between the channels. Therefore the input and the output channels are chosen at the two extremities,

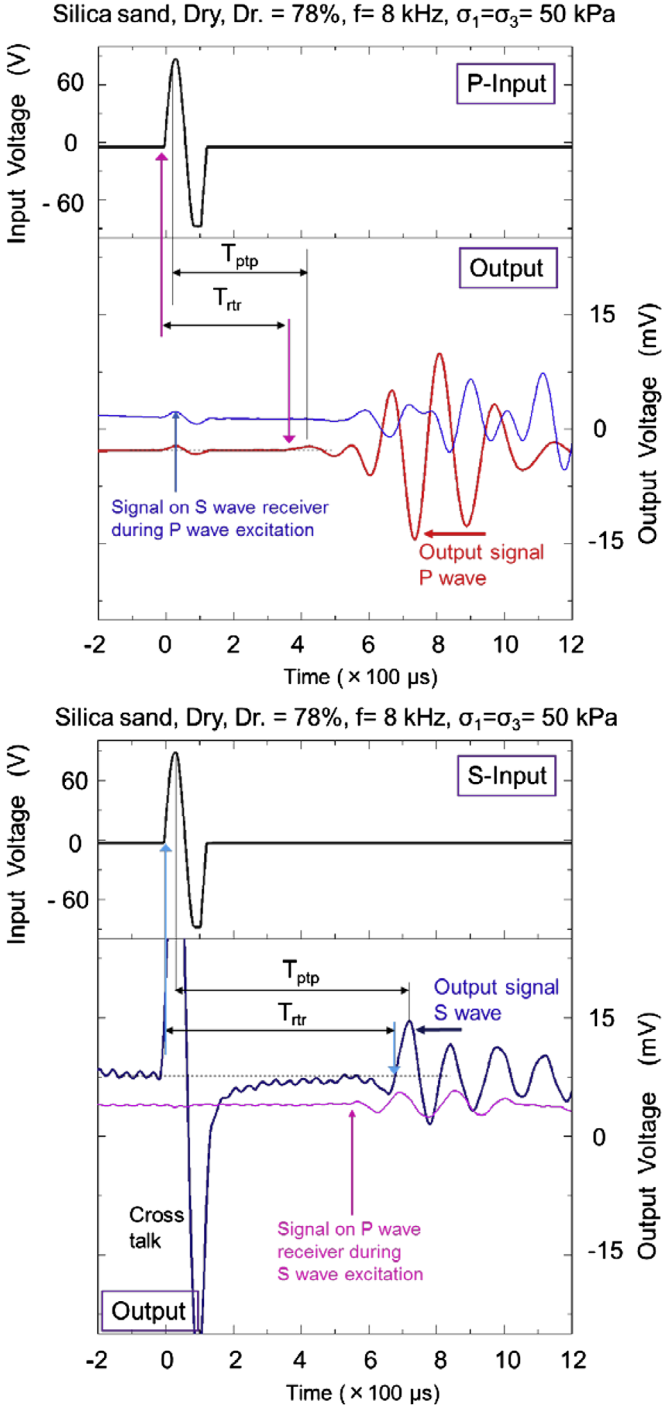

Fig. 17. Typical waveforms achieved on Silica sand at stress level 50 kPa.

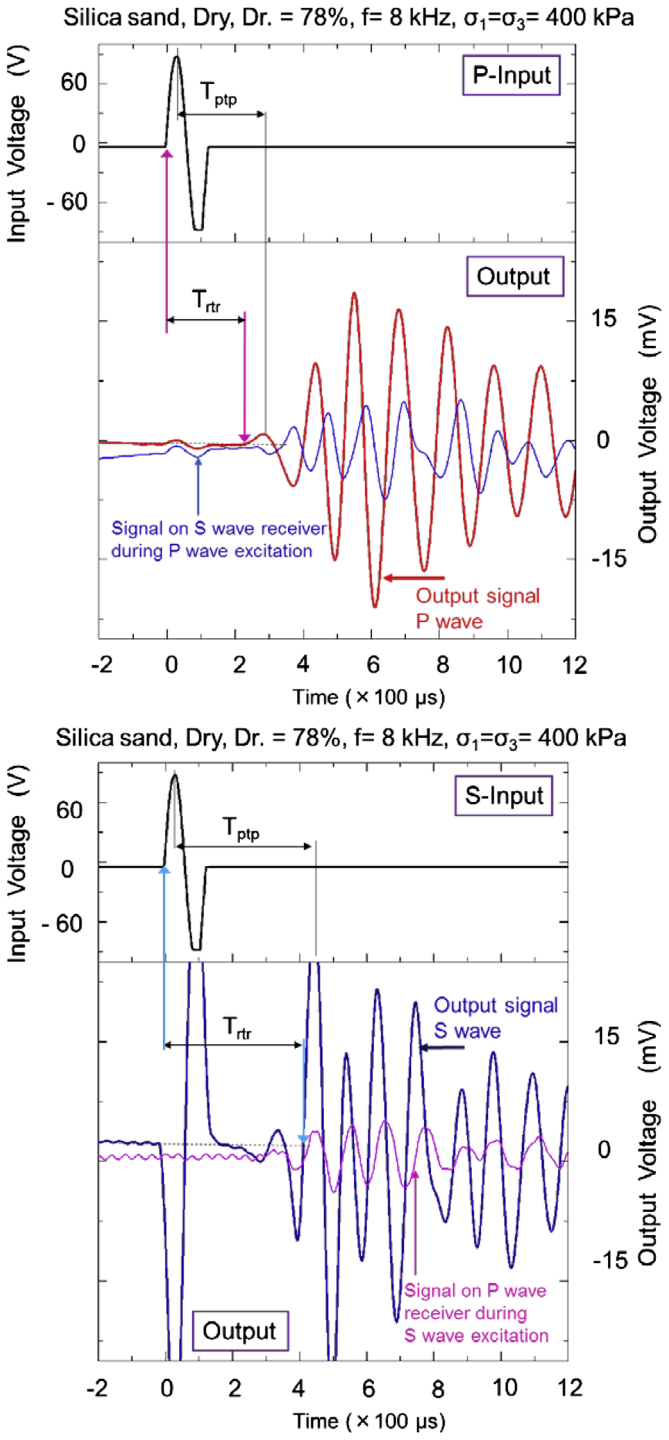

Fig. 18. Typical waveforms achieved on Silica sand at stress level 400 kPa.

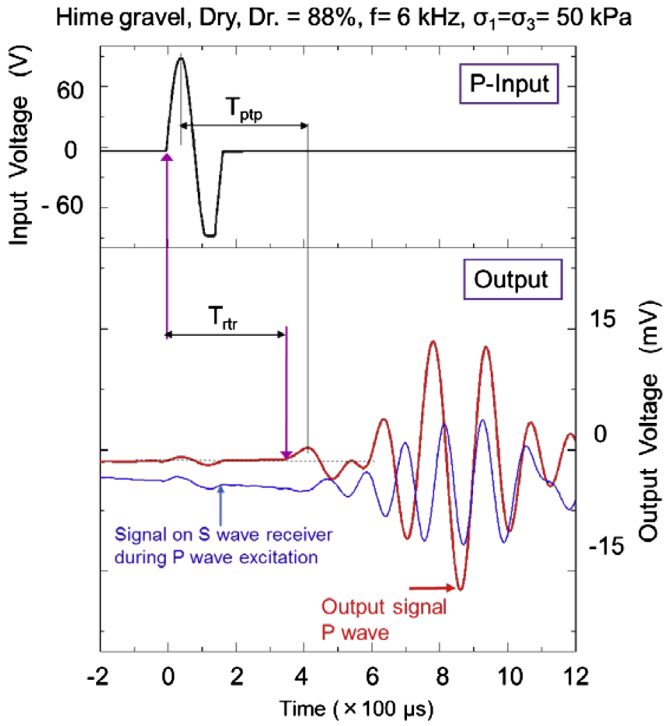

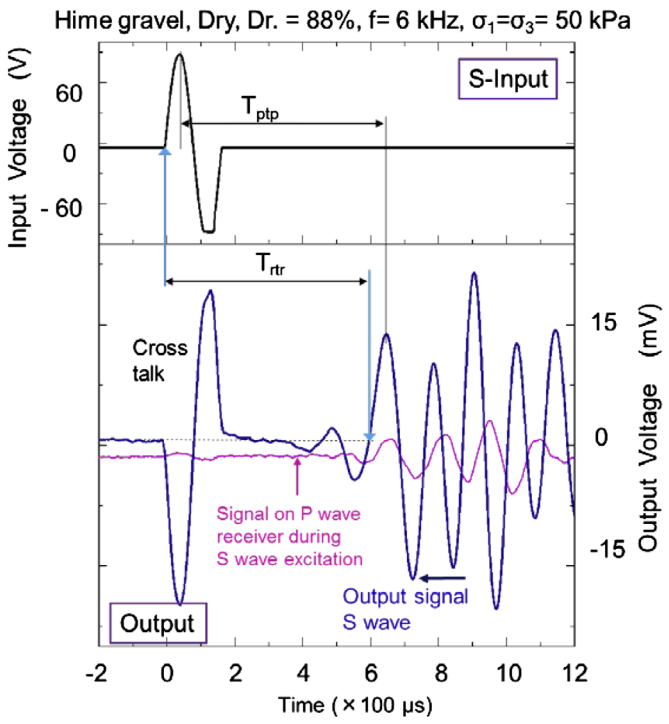

Fig. 19. Typical waveforms achieved on Hime gravel at stress level of 50 kPa.

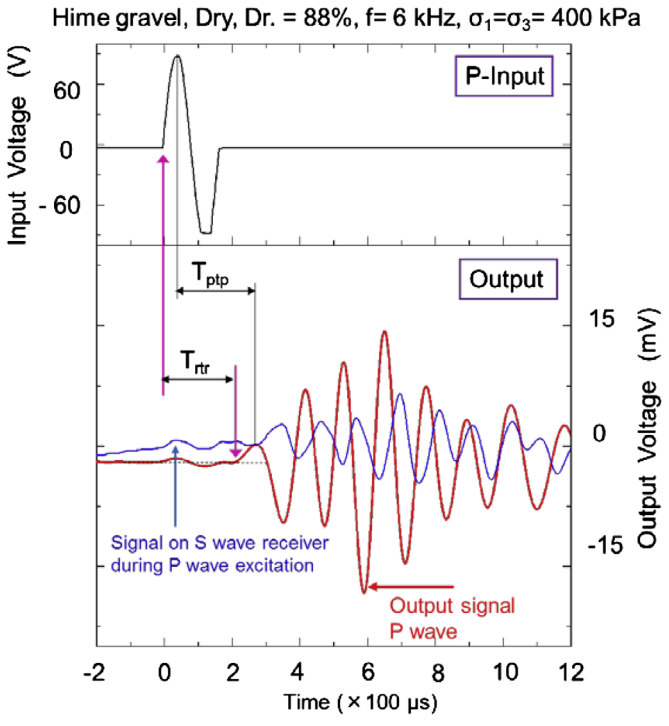

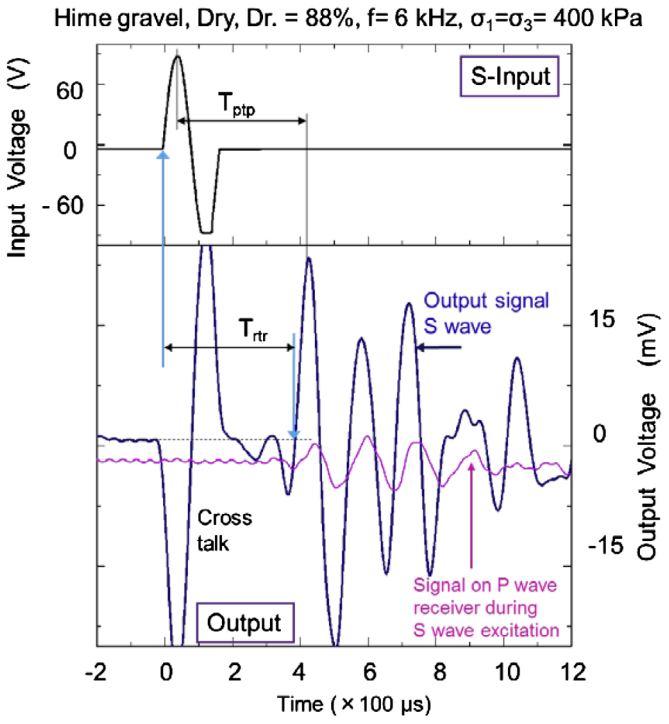

Fig. 20. Typical waveforms achieved on Hime gravel at stress level 400 kPa.

with as much distance between them as possible when an oscilloscope has more than two channels. Still, cross talk could not be completely eliminated, even when all possible efforts were made, including proper grounding and the shielding of the sensors. In Figs. 15–20, the effect of cross talk can be observed in most of the cases, but they are well isolated from the wave arrival point and therefore did not affect the signal interpretation.

The arrival point of signals on the time domain plots are clearly marked for both rising to rising and peak to peak time detection criteria. The time detected by rising to rising of signals and peak to peak of signals is not unique in most cases but the difference is found to be small. In P wave propagation, the time discrepancies between determined by rising to rising of signals and peak to peak of signals were found to be within 10%, as shown in Fig. 21. While concerning with S wave measurement, the time discrepancies were found to be 5%, except for few results of Hime gravel, as displayed in Fig. 22.

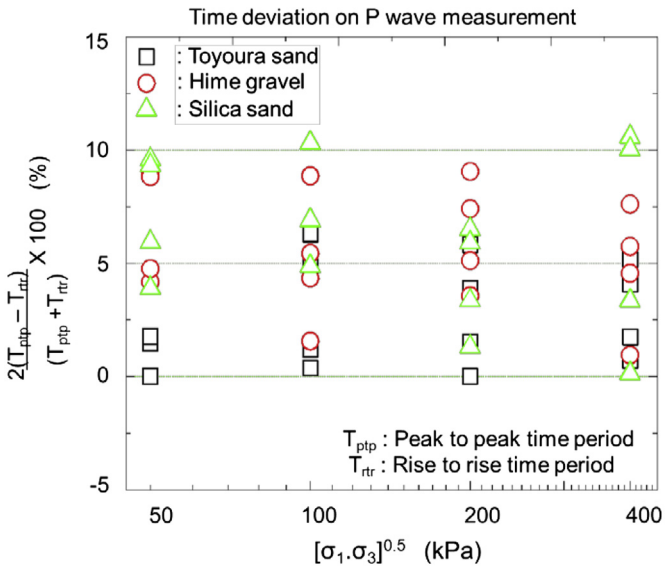

Fig. 21. Discrepancy of time period on P wave measurement.

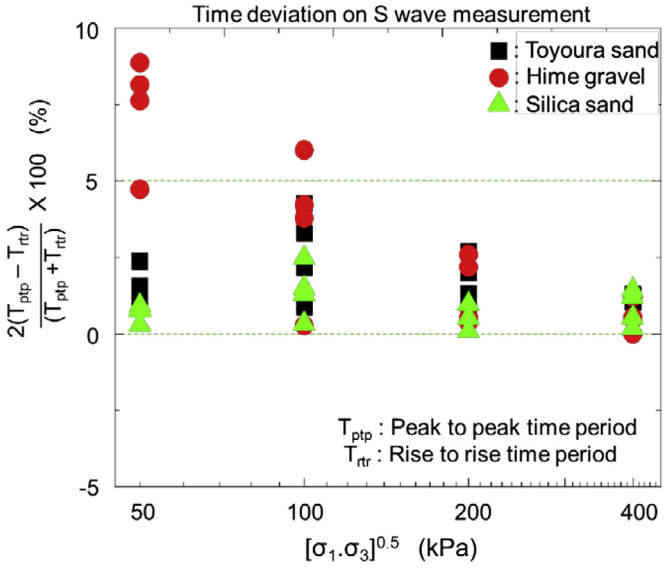

Fig. 22. Discrepancy of time period on S wave measurement.

5. Small strain stiffness evaluation

5.1. Small strain stiffness obtained from triaxial cyclic loading

It is reported that the stiffness at strain level less than 0.001% is nearly elastic for gravels and sands. To evaluate the static small strain stiffness, 11 cyclic loadings with peak to peak strain amplitude up to 0.001% were executed at each stress level. The stress–strain relationship was established with the help of observed stress and deformation data.

Deformation was measured by local deformation transducers (LDTs) developed by Goto et al. (1991) which can measure local strain with high accuracy and free from bedding errors. Stress variation was detected by a load cell installed inside the triaxial cell. Young's modulus (E_{cyc}) was derived by linear

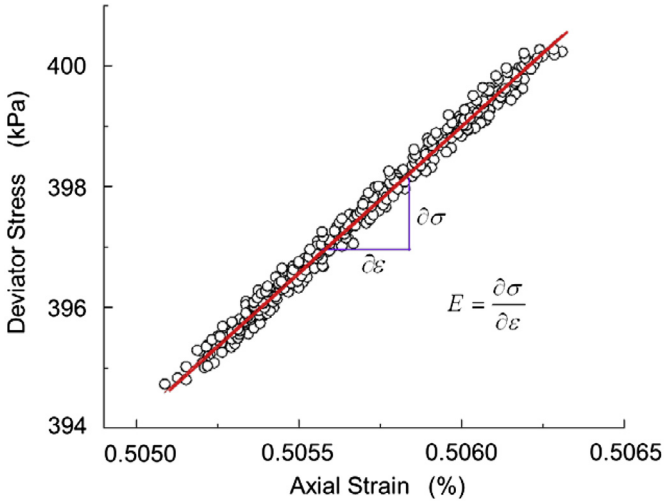

Fig. 23. Example of stress–strain relationship in triaxial cyclic loading.

regression of the data points of the stress–strain cycles. The average value of the stress–strain relation of 5th cycle and 10th cycle was used to evaluate E_{cyc}. The typical plot of stress–strain relation is shown in Fig. 23. The statically evaluated Young's modulus (E) is converted into the shear modulus (G) considering isotropic, homogeneous and elastic material as

$$G = \frac{E}{2(1+\nu)} \tag{1}$$

5.2. Small strain stiffness obtained from wave measurement

Stiffness can be derived from the theoretical relationship with soil density and velocity of propagating wave. The nature of propagating compression waves was considered as a constrained compression wave involving no lateral deformation perpendicular to the direction of wave propagation, as the diameter of soil specimen was relatively large compared to the wave length (Graff, 1991; Khan et al., 2006). The constrained vertical modulus, M, can be achieved by Eq. (2). The constrained modulus was then converted to the unconstrained modulus using Eq. (3). The dynamically obtained shear moduli are computed measuring shear waves directly as Eq. (4). The relation between Young's modulus and the shear modulus is established by Eq. (1) which is used for both static method applying small strain cyclic loadings and wave measurement methods.

$$M = \rho\, V_p^{\,2} \tag{2}$$

$$E = \frac{M(1-2\nu)(1+\nu)}{(1-\nu)} \tag{3}$$

$$G = \rho\, V_s^2 \tag{4}$$

where V_p is the compression wave velocity. V_s is the shear wave velocity, ν is the Poisson's ratio adopted in this study as given in Table 2. The Poisson's ratios used in this study were evaluated by applying static cyclic loadings in all cases, using rectangular specimens for Toyoura sand (Hoque et al., 1998), hollow cylinder

specimens for Hime gravel (De Silva, 2008) and cylindrical specimens for Silica sand (Suwal, in preparation).

5.3. Comparison of small strain stiffness obtained from different methods

Small strain stiffness obtained from disk transducer measurement and from trigger accelerometer method is compared with those obtained from triaxial cyclic loading. In Figs. 24–26, the dynamically evaluated shear moduli are plotted against the statically evaluated shear moduli on Toyoura sand, Silica sand and Hime gravel respectively. The results obtained from the loose and dense specimens are displayed using separate signs. The description of the used notations is

G-DT-P: Shear moduli obtained from P wave measurement using disk transducer method
G-DT-S: Shear moduli obtained from S wave measurement using disk transducer method
G-TA-P: Shear moduli obtained from P wave measurement using trigger accelerometer method
G-TA-S: Shear moduli obtained from S wave measurement using trigger accelerometer method

The results derived by wave measurement are approximately equivalent to those determined by triaxial cyclic loading. The dynamically determined stiffness are scattered along the line with equal static and dynamic results. This shows that the stiffness evaluated by currently proposed disk transducer method tends to be larger than statically determined one, which is consistent with a similarly observation with regard to the stiffness obtained from other types of dynamic measurement (AnhDan et al., 2002; Kuwano and Jardine, 2002). Most of the results obtained by disk transducer ($>80\%$) are found to deviate within 20–50%.

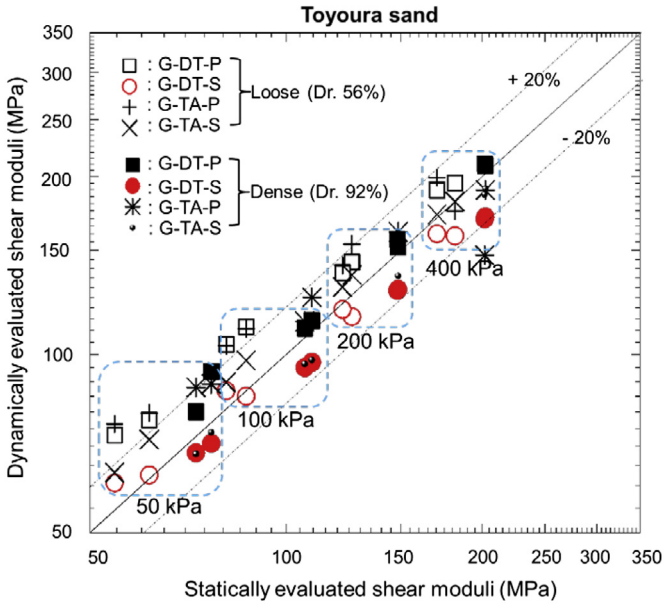

Fig. 24. Statically vs. dynamically evaluated shear stiffness on Toyoura sand.

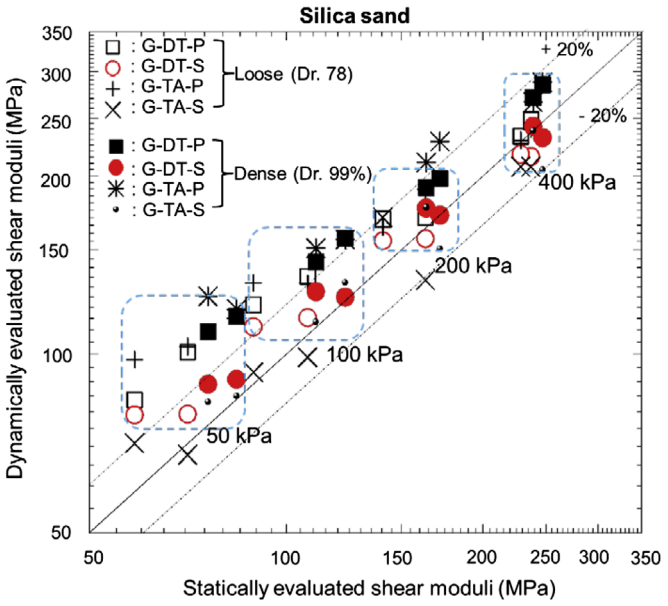

Fig. 25. Statically vs. dynamically evaluated stiffness on Silica sand.

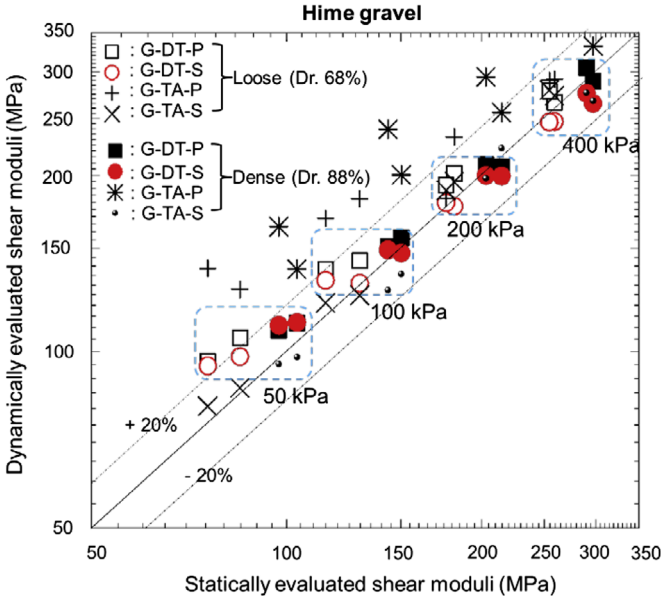

Fig. 26. Statically vs. dynamically evaluated stiffness on Hime gravel.

Errors in the measurement are considered to be caused by various factors, including difficulties in the identification of arrival time of wave, dispersive, anisotropic and non-uniform nature of soil, imperfect coupling between soil and transducer. The deviations of G-DT in percentage are plotted with respect to the stress level for those three geo-materials in Fig. 27. The scatter seems to be smaller in higher confining stresses, possibly reflecting better coupling of soil and transducers in larger stress states. The inherent anisotropy of soil can be also a source of error because its anisotropic nature was neglected when evaluating the small strain stiffness. Kuwano and Jardine (2002) reported that sand can have significant stiffness anisotropy, based on the test results over isotropic and anisotropic stresses obtained from multi-directional bender

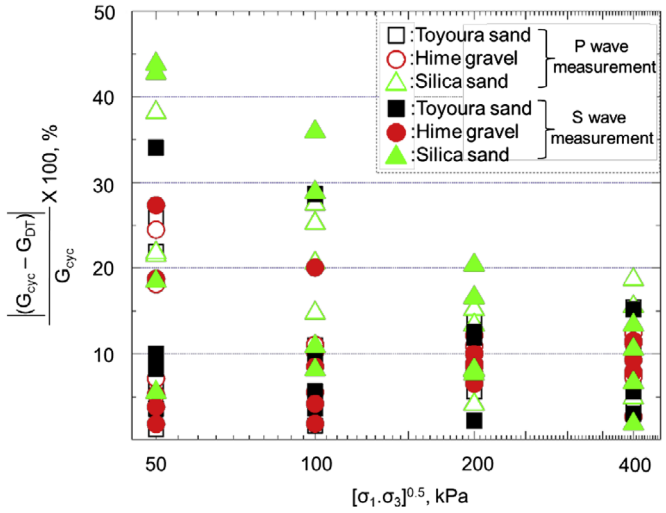

Fig. 27. Stiffness variation with respect to static measurement.

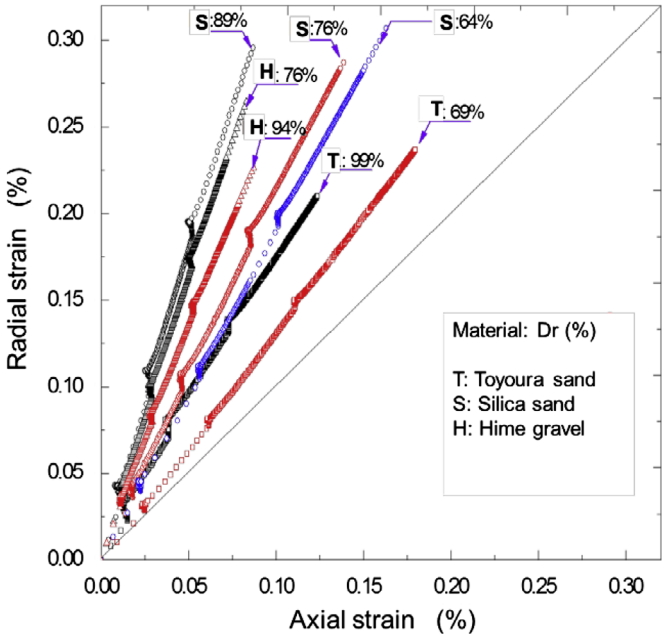

Fig. 28. Deformation anisotropy of tested materials during isotropic consolidation.

element measurement. In this study, we are unable to evaluate stiffness anisotropy from limited test data of only vertical direction of wave propagation. However, since the horizontal deformation was larger than the vertical one during the isotropic consolidation stage, as shown in Fig. 28, it can be assumed that the tested sands exhibit inherent anisotropy in stiffness. The degree of deformation anisotropy seems to be larger for sand with a larger particle size.

6. Conclusions

A disk transducer for elastic wave measurement in laboratory soil specimens has been developed and its performance and applicability on sands are described.

The disk transducer is capable of measuring both P and S waves in a soil specimen. The disk transducer does not need to be inserted into the specimen, so it is free from the difficulties of preserving the integrity of the material around the transducer. However, a good contact between the surface of the transducer and the tested specimen is required, and this study aims to confirm that the disk transducer may be applied to a coarse grained material, when the diameter of the disk transducer is more than 10 times of mean diameter of the tested materials. In S wave propagation when using this equipment, it was noted that the waves in a certain frequency range (in this case approximately 10–20 kHz) were not able to be successfully transmitted. The S wave measurement using the disk transducer in this study was therefore recommended to perform with frequencies less than 8 kHz. The wave velocities obtained by the disk transducer method are converted to small strain shear stiffness and compared with those obtained from trigger accelerometer method and triaxial cyclic loading, on the assumption that the stiffness of tested materials are isotropic. The disk transducer method shows a promise of equivalent performance to the other tested methods and scatters between the disk transducer method and triaxial cyclic loading are mostly within 20–50%. The disk transducer is a promising technique that can be further explored in the future for wave measurements in laboratory soil specimens.

Acknowledgments

We greatly appreciate Mr. Takeshi Sato of Integrated Geotechnology Institute Ltd., who provided valuable and kind advice in the development of the transducer, and Mr. Sarju Mulmi, a former graduate student of the University of Tokyo, who provided his assistance at the primary stage of the development.

References

Ackerley, S.K., Hellings, J.E., Jardine, R.J., 1987. Discussion on a new device for measuring local axial strain strains on triaxial specimens. Geotechnique 37 (3), 413–417.

AnhDan, L. Q., Koseki, J., and Sato, T., 2002. Comparison of Young's Moduli of Dense Sand and Gravel Measured by Dynamic and Static Methods. Geotechinical Testing Journal, 25(4), 349-368.

Alvarado, G., Coop, M.R., 2011. On the performance of bender elements in triaxial tests. Géotechnique, 62 (1), http://dx.doi.org/10.1680/geot.7.00086 (Available online: 8 August 2011).

Amaral, M., Viana da Fonseca, A., Arroyo, M., Cascante, G., Carvalho, J.M., 2011. Compression and shear wave propagation in cemented-sand specimens. Géotechnique Letters (ICE Publication) 1, http://dxdoi.org/10.1680/geolett.11.00032.

AnhDan, L.Q., Koseki, J., Sato, T., 2002. Comparison of Young's moduli of dense sand and gravel measured by dynamic and static methods. Geotechinical Testing Journal 25 (4), 349–368.

Arroyo, M., Wood, D.M., Greening, P.D., 2003. Source near-field effects and pulse tests in soil samples. Geotechnique 53 (3), 337–345.

Arroyo, M., Muir Wood, D., Greening, P.D., Medina, L., Rio, J., 2006. Effects of sample size on bender-based axial G0 measurements. Geotechnique 56 (1), 39–52.

Arulnathan, R., Boulanger, R.W., Riemer, M.F., 1998. Analysis of Bender element tests. Geotechnical Testing Journal 21 (2), 120–131.

Blewett, J., Blewtt, I.J., Woodward, P.K., 1999. Measurement of shear-wave velocity using phase sensitive detection technique. Canadian Geotechinical Journal 36 (5), 934–939.

Brignoli, E.G.M., Gotti, M., Stokoe II, K.H., 1996. Measurement of shear waves in laboratory specimens by means of piezoelectric transducers. Geotechnical Testing Journal 19 (4), 384–397.

Burland, J.B., Symes, M., 1982. A simple axial displacement gauge for use in triaxial apparatus. Geotechnique 32 (1), 62–65.

Burland, J.B., 1989. Ninth Laurits Bjerrum memorial lecture: small is beautiful—the stiffness of soils at small strain. Canadian Geotechnical Journal 26 (4), 499–516.

Camacho-Tauta, J., Santos, J.A., Viana da Fonseca, A., 2008. Evaluation of the Small-Strain Shear Modulus Using Two Bender-Receivers and a Controlled External Source, Deformational Characteristics of Geomaterials. vol. 2. IOS Press, Atlanta, GA703–709.

Clayton, C.R.I., Khatrush, S.A., 1986. A new device for measuring local axial strains on triaxial specimens. Géotechnique 36 (4), 593–597.

De Silva, L.I.N., 2008. Deformation Characteristics of Sand Subjected to Cyclic Drained and Undrained Torsional Loadings and there Modeling (Ph. D. thesis). The University of Tokyo.

Di Benedetto, H., Tatsuoka, F., 1997. Small strain behavior of geomaterials: modelling of strain rate effects. Soils and Foundations 37 (2), 127–138.

Duttine, A., Di Benedetto, H., Pham Van Bang, D., Ezaoui, A., 2007. Anisotropic small strain elastic properties of sands and mixture of sand–clay measured by dynamic and static methods. Soils and Foundations 47, 457–472.

Goto, S., Tatsuaka, F., Shibuya, S., Kim, Y.-S., Sato, T., 1991. A simple gauge for local small strain measurements in the laboratory. Soils and Foundations 31 (1), 169–180.

Graff, K.F., 1991. Wave Motion in Elastic Solids. Dover, Oxford, UK.

Greening, P.D., Nash, D.F.T., 2004. Frequency domain determination of Go using bender elements. Geotechnical Testing Journal 27 (3), 288–294.

Hicher, P.Y., 1996. Elastic properties of soils. Journal of Geotechnical Engineering 122 (8), 641–648.

Hird, C.C., Yung, P.C.Y., 1989. The use of proximity transducers for local ;strain measurements in triaxial tests. Geotechnical Testing journal 12 (4), 292–296.

Hoque, E., Tatsuoka, F., Sato, T., 1998. Measuring anisotropic elastic properties of sand using a large triaxial specimen. Geotechnical Tesintg Journal, GTJODJ 19 (4), 411–420.

Ismail, M.A., Rammah, K.I., 2005. Shear-plate transducers as a possible alternative to bender elements for measuring G_{max}. Géotechnique 55 (5), 403–407.

Jamiolkowski, M., Lancellotta, R., Lo Presti, D.C.F., 1995. Remarks on the stiffness at small strains of six Italian clays. In: Shibuya, S. (Ed.), Pre-Failure Deformation of Geomaterials. Balkema, pp. 817–836.

Jardine, R.J., Symes, M.J., Burland, J.B., 1984. Measurements of Soil stiffness in the triaxial apparatus. Geotechnique 34 (3), 323–340.

Jovicic, V., Coop, M.R., Simic, M., 1996. Objective criteria for determining G_{max} from bender element tests. Geotechnique 46 (22), 357–362.

Khan, Z., Majid, A., Cascante, G., Hutchinson, D. J., and Pezeshkpour, P., 2006. Characterization of a cemented sand with the pulse-velocity method. Canadian geotechnical journal, 43(3), 294-309. DOI:10.1139/t06-008.

Khan, Z., Cascante, G., El-Naggar, H., 2011. Dynamic properties of cemented sands using ultrasonic waves. Canadian Geotechnical Journal 48 (1), 1–15.

Kumar, J., Madhusudhan, B.N., 2010. Effects of relative density and confining pressure on Poisson ratio from bender and extender elements tests. Geotechnique 60 (7), 561–567.

Kuwano, R., Jardine, J.R., 2002. On the applicability of cross-anisotropic elasticity to granular materials at very small strains. Geotechnique 52 (10), 727–749.

Kuwano, R., Wicaksono, R.I., Mulmi, S., 2008. Small strain stiffness of coarse granular materials measured by wave propagation. In: Proceedings of the 4th International Symposium on Deformation Characteristics of Geomaterials, IS-Atlanta 2008, vol. 2, pp. 749–756.

Lee, C., Truong, Q.H., Lee, J.S., 2010. Cementation and bond degradation of rubber-sand mixtures. Canadian Geotechnical Journal 47, 763–774.

Lee, J.-T., Tien, K.-C., Te, O.Y., Huang, A-B, 2011. A fiber optic sensored triaxial testing device. ASTM Geotechnical Testing Journal 34 (2), 1–9.

Lee, J.S., Sanatamarina, J.C., 2005. Bender elements: performance and signal interpretation. Journal of Geotechnical and Geo-environmental Engineering 131 (9), 1063–1070.

Leong, E.C., Cahyadi, J., Rahardjo, H., 2009. Measuring shear and compression wave velocities of soil using bender-extender elements. Canadian Geotechnical Engineering Journal 46, 792–812.

Lo Presti, D., Pallara, O., Lancelotta, R., Amandi, M., Maniscalco, R., 1993. Monotonic and cyclic loading behavior of two sands at small strains. Geotechnical Testing journal 16 (4), 409–424.

Mulmi, S., 2008. Small Strain Stiffness Measurement of Geo-materials by Elastic Waves (Master thesis). Department of Civil Engineering, The University of Tokyo, Japan.

Pallara, O., Mattone, M., Lo Presti, D.C.F., 2008. Bender elements: bad source—good receiver. In: Proceedings of the 4th international symposium on deformation characteristics of geomaterials, IS-Atlanta 2008, vol. 2, pp. 697–702.

Pineda, J.A., Arroyo, M., Romero, E., Alonso E.E., 2008. Dynamic tracking of hydraulically induced clay stone degradation. In: Proceedings of the 4th International Symposium on Deformation Characteristics of Geomaterials, IOS Press, pp. 809–817.

Richart, F.E., Hall, J.R., Woods, R.D., 1970. Vibrations of Soils and Foundations. Prentice Hall, Englewood Cliffs, NJ.

Rio, J., Greening, P., Medina, L., 2003. Influence of sample geometry on shear wave propagation using bender elements. In: Proceedings of Deformation Characteristics of Geomaterials, Lyon, France, 22–24 September, Balkema, Lyon, France, pp. 963–967.

Shirley, D.J., Hampton, L.D., 1978. Shear-wave measurements in laboratory sediments. Journal of Acoustical Society of America 63, (2).

Sachse, W., Pao, Y.-H., 1978. On the determination of phase and group velocities of dispersive waves in solids. Journal of Applied Physics 49 (8), 4320–4327.

Stokoe, K.H., Hoar, R.J., 1978. Field measurement of shear wave velocity by cross hole seismic methods. In: Proceedings of the Conference on Dynamic Methods in Soil and Rock Mechanics, vol. 3, Karlsruhe, Germany, pp. 115–137.

Stokoe, K.H., II, Santamarina, J.C., 2000. Seismic-wave-based testing in geotechnical engineering. In: Plenary Paper, International Conference on Geotechnical and Geological Engineering, GeoEng 2000. Melbourne, Australia, pp. 1490–1536.

Suwal, L.P., Kuwano,R., Ebizuka,H., Sato,T., 2009. Performance of plate transducer—transducer for dynamic measurement in laboratory specimens. In: Proceedings of 11th International Summer Symposium, International Activities Committee, JSCE, pp. 113–116.

Suwal, L. P., 2013. Disk Transducer for Elastic Wave Measurement and Its Application to Unsaturated Sandy Soils. Ph.D. Thesis, the University of Tokyo.

Tallavó, F., Cascante, G., Pandey, M.D., 2011. Ultrasonic transducers characterisation for evaluation of stiff geomaterials. Géotechnique 61 (6), 501–510.

Tatsuoka, F., Kohata, Y., 1995. stiffness of Hard soils and soft rocks in engineering applications. In: Shibuya, S. (Ed.), Keynote Lecture, Proceedings of the International Symposium Pre-failure Deformation of Geomaterials, vol. 2. Balkema, pp. 947–1063.

Tatsuoka, F., Shibuya, S., 1992. Deformation characteristics of soils and rocks from field and laboratory tests. In: Proceedings of the 9th Asian Regional Conference of SMFE, vol. 2. Bangkok, pp. 101–170.

Tatsuoka, F., Teachavorasinsun, S., Dong, J., Kohata, Y., Sato, T., 1994. Importance of measuring local strains in cyclic triaxial tests on granular materials. In: Ebelhar, R., Drnevich, V., Kutter, B. (Eds.). Dynamic Geotechnical Test II, ASTM international STP 1213, Philadelphia, p. 432. http://www.astm.org/BOOKSTORE/PUBS/STP1213.htm.

Viggiani, G., Atkinson, J.H., 1995. Interpretation of Bender element tests. Geotechnique 45 (1), 149–154.

Viana da Fonseca, A., Ferreira, C., Fahey, M., 2009. A framework interpreting bender element testing. Combining time-domain and frequency domain methods. Geotechnical Testing Journal 32 (2), 91–107.

Yamashita, S., Kawaghchi, T., Nakata, Y., Mikami, T., Fujiwara, T., Shibuya, S., 2009. Interpretation of international parallel test on the measurement of G_{max} using bender elements. Soils and Foundations 49, 631–650.